

Emergent dynamics and spatiotemporal patterns in soft robotic swarms

R. Pramanik^{1,2}, R.W.C.P. Verstappen¹ and P.R. Onck^{2,*}

¹*Computational & Numerical Mathematics Group, Bernoulli Institute for Mathematics,
Computer Science & Artificial Intelligence, University of Groningen, Netherlands*

²*Micromechanics Group, Zernike Institute for Advanced Materials, University of Groningen, Netherlands*

(Dated: October 1, 2024)

The collective swimming of soft robots in an infinite viscous fluid is an emergent phenomenon due to the non-reciprocal hydrodynamic interactions between individual swimmers. These physical interactions give rise to unique spatiotemporal patterns and unusual swimming trajectories that are often difficult to predict due to the two-way fully coupled nature of the strong fluid-structure interaction at a thermodynamic state that is far from equilibrium. Until now, robotic swarms have mostly been studied for rigid swimmers in two-dimensional settings. Here we study the emergence of three-dimensional spatiotemporal patterns of helical magnetically actuated soft-robotic swimmers by systematically studying the effect of different initial configurations. Our results show that swimmers with variations in initial positions in the swimming direction are attracted to each other, while swimmers with variations in lateral positions repel each other, eventually converging to a state in which all swimmers concentrate in one lateral plane drifting radially outward.

I. INTRODUCTION

The study of active matter has gained significant attention in recent years due to its diverse applications across biological systems, discrete materials, and synthetic structures [1–3]. This includes granular matter, bacterial swarms, flocking behaviors, and stimuli-responsive gels, all of which exhibit complex, far-from-equilibrium self-organization driven by hydrodynamic interactions [4–6]. Within this context, systems such as magnetotactic bacteria and swimming cells demonstrate non-reciprocal fluid-mediated interactions that lead to emergent behaviors like vortex formation and viscous merging [7–9]. These phenomena are not only theoretically intriguing but also have practical implications in the development of advanced microrobotic systems [10].

Focusing on the burgeoning field of magnetically actuated microrobotics, there is a growing interest in using magnetic fields to control and actuate micro- and nanoscale robotic swarms for biomedical applications. These systems offer promising solutions for targeted drug delivery, minimally invasive surgeries, and parallelized manipulation in medical settings [11, 12]. Recent advances have demonstrated various locomotion modes - such as rolling, flipping, and corkscrew motions - enabled by magnetic actuation, which are particularly useful in navigating complex biological environments [13, 14]. Among these, rotating magnetic field-driven microrobots have shown great potential, especially in applications requiring precise control and localization. For instance, kinematic models have been developed to predict the behavior of magnetic screws in soft tissues, and reconfigurable collective modes of magnetically actuated disks have been explored, paving the way for innovative biomedical interventions [15, 16].

Theoretical models have been proposed to study the collective behavior of miniaturized swarms [17]; e.g., control of emergent robotic systems has been reported using Smooth Particle Hydrodynamic (SPH) models [18]. The collective motion of magnetic spinners and rollers has been studied using mathematical models for the swarm particles that were subjected to magnetic torques based on Maxwell’s equations [19]. The hydrodynamic states were reported to capture the two-dimensional collective behavior of self-assembled spinners at the water-air interface [20]. Another study on robot-robot interactions has been proposed to predict the evolution of swarm macroscopic properties (such as separation, compressibility, and cohesivity) based on SPH control of robotic swarms [21].

Recently, spinning magnetic micron-sized disks has been shown to self-organize at the air-water interface under rotating external magnetic fields to generate various spatiotemporal patterns based on an appropriately defined interaction potential [22]; here, the local pairwise interactions (between two disks) induced global patterns. In addition, the collective spatial behavior was shown to depend on the external actuation frequency based on patterns produced from Monte Carlo simulations [23]. Swarms of ferromagnetic microparticle ensembles at the air-water interface were subjected to a uniaxial oscillating magnetic field that lead to self-organization and clustering [24]. While the particle dynamics was described using a lattice spring model (where a network of Hookean springs connect point masses), the two-dimensional fluid dynamics as well as the fluid-structure interactions were captured by the lattice Boltzmann model [25–27].

Although praiseworthy achievements have been made in the field of microrobotic swarms, these have only been reported for two-dimensional in-plane (hydrodynamic) systems of rigid swimmers, such as spheres [28], rollers [29], spinners [19], particles [30], disks [31] and colloids [32]. However, it is important to note that these rigid robots suffer large setbacks with system miniaturization,

* Corresponding author: p.r.onck@rug.nl

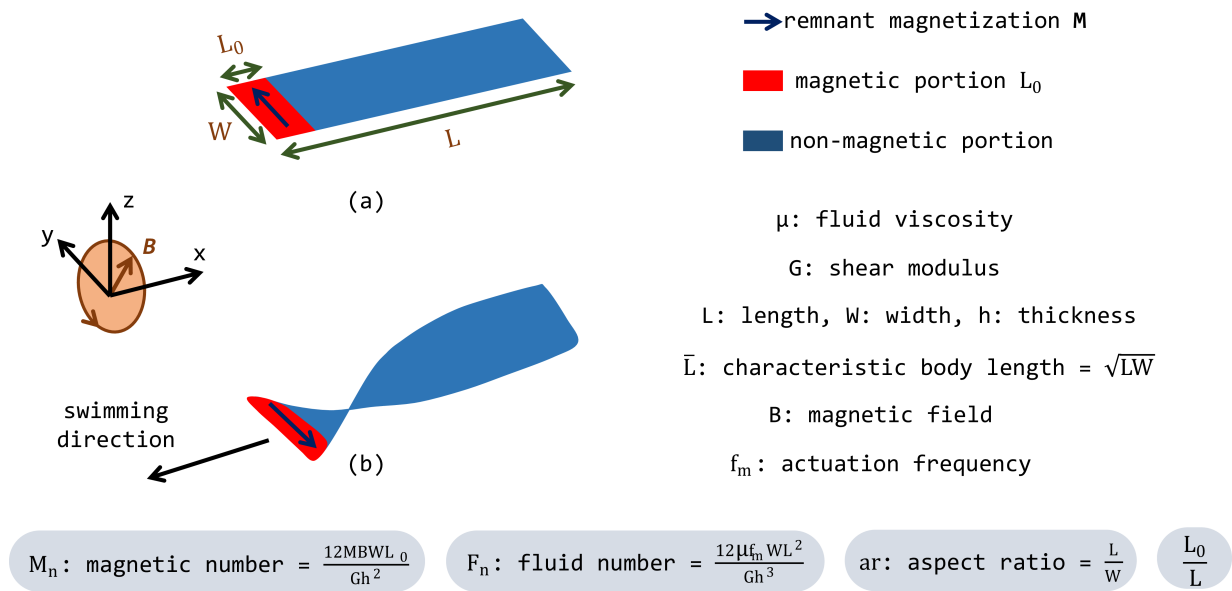


FIG. 1: (a) Schematic illustration of a partially magnetic soft robotic swimmer exposed to an external magnetic field. (b) Propulsion is generated by applying an external uniform rotating magnetic field B with the rotation axis aligned along the x -axis. Chirality is naturally formed on-the-fly as a result of the interplay between viscous drag forces acting on the entire swimmer and magnetic body torques concentrated on one end of the swimmer (multimedia available online).

resulting in reduced swimming modalities that hinder their applicability in biomedical applications. Additionally, precise path control, maneuverability, and localization of these rigid magnetic swarms is quite difficult. To overcome this, magnetic soft robotic swimmers have been developed, demonstrating improved swimming techniques, reliable path control, precise localization, and adaptive swimming behavior [33–40]. However, the operation of these inherently soft, magnetically deformable swimmers under three-dimensional swarming conditions has not been explored before. Here, we study the emergent behavior and collective swimming of miniaturized magnetically actuated soft robotic swimmers [41, 42], where the individual swimmers communicate with each another through long-range hydrodynamic interactions in a three-dimensional setting. We will study how different initial spatial configurations, specifically in-plane and out-of-plane arrangements, affect the emergent behavior and collective swimming dynamics. For this we use a fully coupled computational model that integrates fluid dynamics, solid mechanics, large deformation solid-fluid interaction, and magnetics in a unified framework [43].

The paper is structured as follows: we begin by validating the numerical convergence of our model for configurations involving one and two helical swimmers. We then present findings on the emergent behavior of two swimmers with different initial configurations in a three-dimensional setting. Additionally, we examine the spatiotemporal patterning and collective swimming dynamics of three helical swimmers, with particular attention to their relative spacing as a function of cycle number. We

discuss how the aspect ratio of the swimmers influences their collective swimming and corresponding trajectories and we close with a summary and conclusions.

II. RESULTS & DISCUSSION

For the present study, we consider partially magnetized elastica that are membrane-like and shaped in the form of rectangular flaps with only one end magnetized [see Fig. 1 (multimedia available online)] [44]. By applying an external rotating magnetic field, magnetic torques are applied at the magnetic end, while the passive (i.e., non-magnetic) portion is subjected to drag forces from the surrounding fluid. Therefore, as a natural consequence of fluid-structure interaction in combination with the localized magnetic body torque, these swimmers develop a chirality (twisted body profile) and propel through the fluid using a typical corkscrew motion. Due to their miniaturized length scales, the Reynolds number of the flow is approximately equal to zero (Stokes flow). We use a robust fully coupled computational model (that simultaneously accounts for solid mechanics, fluid dynamics, large deformation fluid-structure interaction, and magnetics in a monolithic manner [43]) to study the emerging behaviour of magnetically actuated helical soft robotic swimmer collectives involving two-way fluid-structure interactions as well as hydrodynamic effects. For all our simulations, we consider the magnetic (M_n) and fluid (F_n) numbers to have values of 50 and 5, respectively (refer [44] for details); the default value of f_m is chosen

as 5Hz.

A. Numerical convergence: 1 swimmer

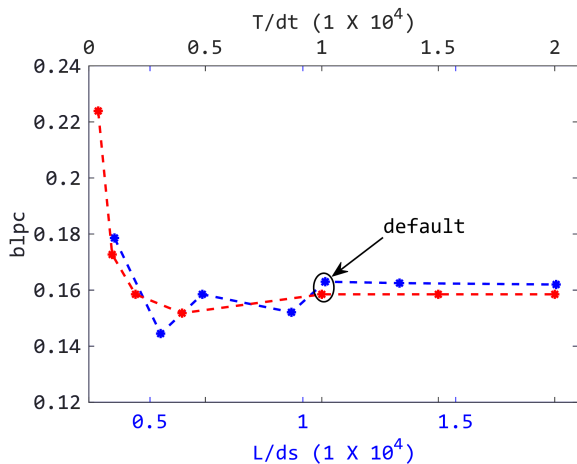


FIG. 2: Convergence study and the default values corresponding to dt (in red) and ds (in blue) chosen for further simulations henceforth.

We begin with the numerical convergence study to ensure the robustness and stability of the computational framework, and also fix our default values of time step (dt) and mesh size (ds). For the convergence test, a magnetically actuated helical soft robotic swimmer is subjected to rotating magnetic fields to achieve a steady-state swimming speed reported in body lengths per cycle, $blpc = c/\bar{L}f_m$ with c the average swimming speed, \bar{L} the characteristic body length, and f_m the actuation frequency. We plot the spatial and temporal convergence results in Fig. 2 with $T=1/f_m$. We observe that while the former has an oscillatory convergence behavior, the latter has a monotonic convergence. Furthermore, the default values of ds and dt have been denoted, and these are used for all simulations henceforth.

B. Numerical convergence: 2 swimmers

We now report the swimming trajectories of 2 swimmers that are initially spaced two bodylengths (bl) apart along the z -axis; their initial configuration is schematically shown in Fig. 3 with swimmer 1 ($s1$) at $(y,z) = (0,1)$ and swimmer 2 ($s2$) at $(y,z) = (0,3)$. Remarkably, while these swimmers propel along the negative x -axis using helical propulsion (and maintaining a steady shape profile) due to the application of (constant in magnitude and) rotating magnetic field in the y - z plane, we observe that they additionally start revolving around each other due to hydrodynamic interactions (multimedia available online).

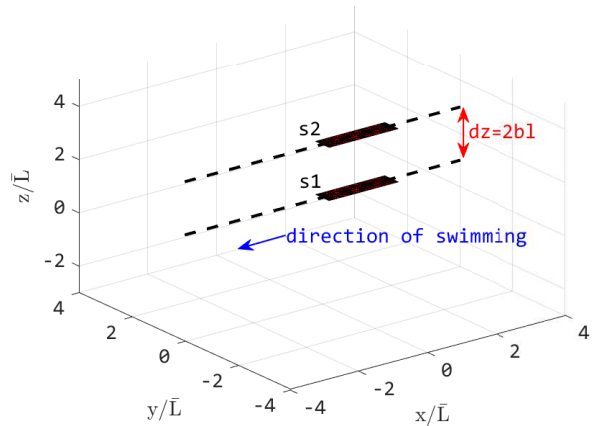


FIG. 3: Schematic representation of initial (spatial) configurations of two soft robotic swimmers chosen for numerical convergence of the effect of hydrodynamic interactions for different values of ds and dt .

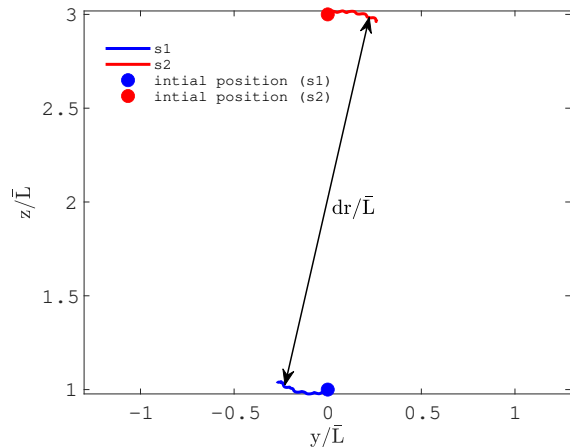


FIG. 4: Phase plot of the two swimmers with initial condition as Fig. 3 that shows their swimming trajectories and starting positions.

We report their swimming trajectories (phase plots) and the normalized lateral separation (drift dr/\bar{L}) in the y - z plane (to completely understand and quantify the hydrodynamic interactions between them). To further validate our numerical framework, we study this example for different values of dt (see Fig. 5) and ds (see Fig. 6). Note that we plot the phase plots only for swimmer $s1$ (for the sake of clarity). Owing to symmetry, the trajectory of swimmer $s2$ would be alike. We observe that the choice of different time steps does not have a huge influence on either the phase plot (Fig. 5a) or the lateral drift (Fig. 5b). Two length scales appear in the phase plot; while we attribute the smaller length scale to the typical wiggling motion of the geometric center of the helical swimmer itself, the larger length scale represents

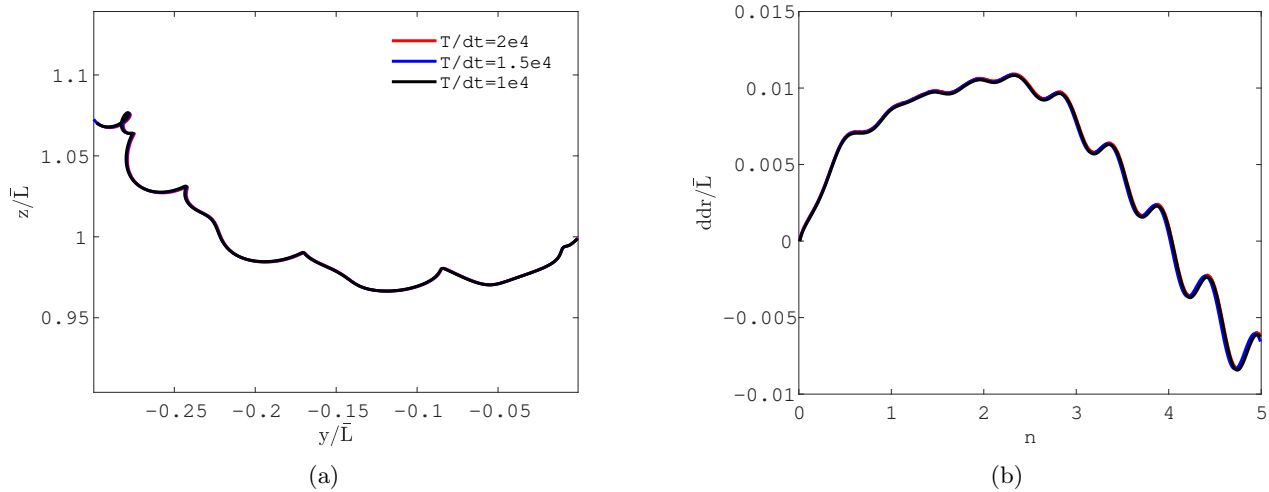


FIG. 5: (a) Phase plot and (b) variation of lateral drift with an increase in the number of swimming cycles, n . Numerical convergence test of 2 swimmers for different time steps, dt and a mesh size $ds=L/1 \times 10^4$.

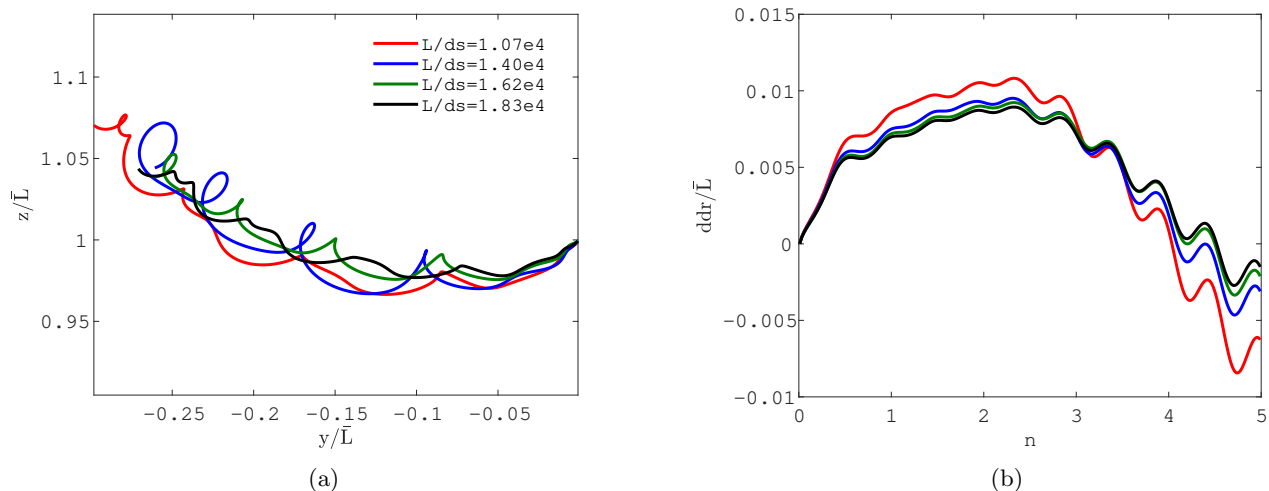


FIG. 6: (a) Phase plot and (b) variation of lateral drift with an increase in the number of swimming cycles, n . Numerical convergence test of 2 swimmers for different mesh sizes, ds and a time step $dt=T/1 \times 10^4$.

the circular path traversal of the swimmers, see Fig. 6b. These two length scales could interact in order to generate a third length scale (as we shall later see for robots of different aspect ratios).

C. Emergent behavior: 2 swimmers

Now, we systematically consider different in-plane and out-of-plane configurations to study the effect of initial arrangement (spatial orientation) upon their collective swimming, spatiotemporal patterning, and emergent behavior. First, we study the 2-swimmer swarm that are spaced a few bodylengths (bl) apart along either the x - or z -axis (see Fig. 7). Due to location motion direction

into the x -axis and the angular motion in the y - z plane, a spacing in the y -direction is similar to a spacing in the z -direction. We define dr/\bar{L} as the normalized lateral separation between the swimmers, while ddr/\bar{L} measures the change in dr/\bar{L} to represent the lateral drift. Furthermore, we have similar notations for axial separation: dx/\bar{L} , and ddx/\bar{L} represents the normalized axial separation and change in axial separation between the swimmers, and so on. Note that we report non-dimensional kinematic quantities such as phase plots, axial approach (ddx/\bar{L}) and lateral drift (ddr/\bar{L}) as a function of number of actuation cycles (n) to ensure a uniform comparison of their swimming trajectories and spatiotemporal patterning.

Four different starting configurations are considered:

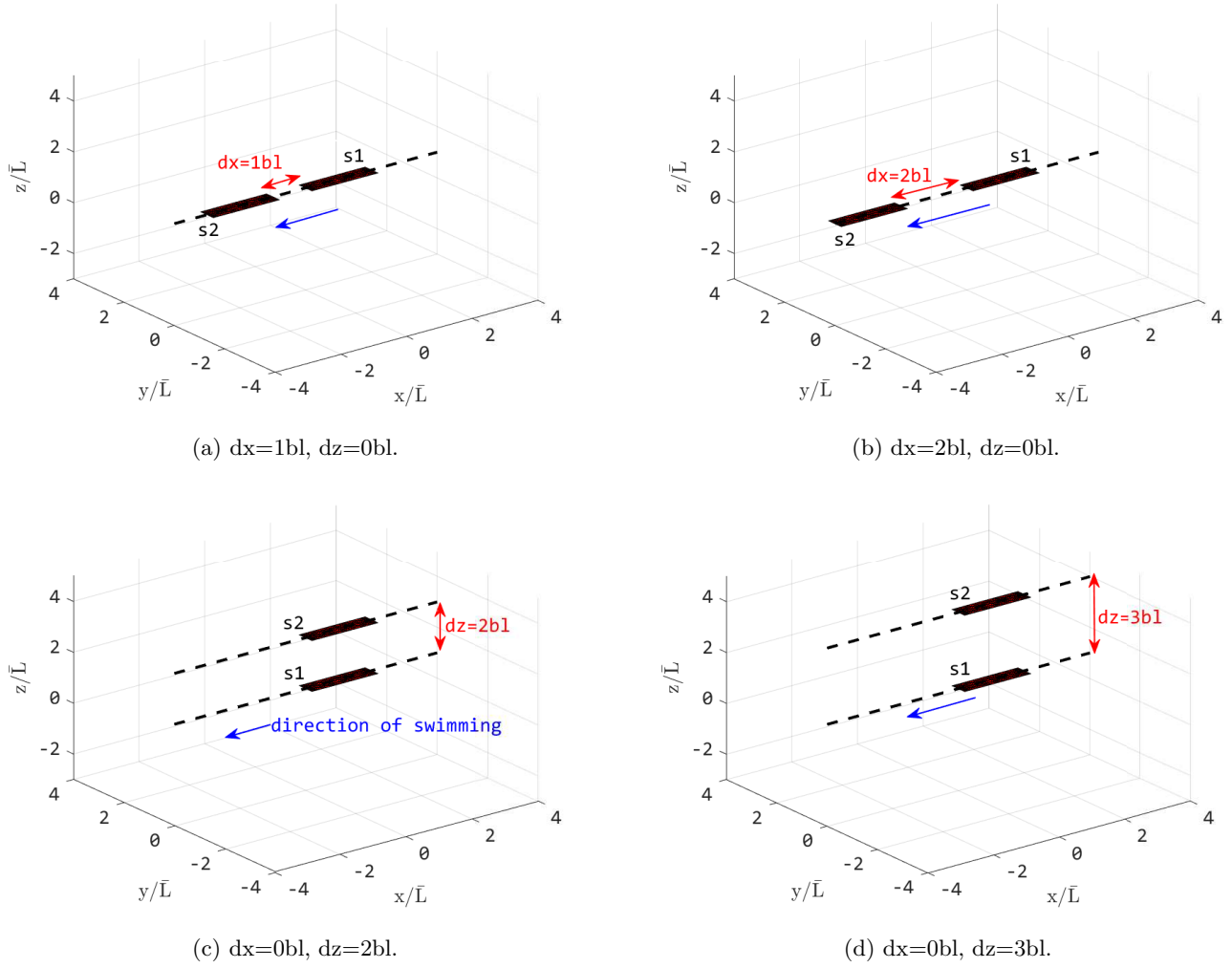


FIG. 7: Schematic representation of different initial (spatial) configurations of two soft robotic swimmers. Swimmers $s1$ and $s2$ are identified in black. The direction of swimming is shown in blue. The separation between the swimmers is denoted as either dx or dz in red. The front of swimmer $s1$ in all subplots is located at $(x,y,z) = (0,0,\bar{L})$; for (a) and (c): (multimedia available online).

(a) $dx=1bl$, $dz=0bl$ [Fig. 7a (multimedia online)], (b) $dx=2bl$, $dz=0bl$ (Fig. 7b), (c) $dx=0bl$, $dz=2bl$ [Fig. 7c (multimedia online)], and (d) $dx=0bl$, $dz=3bl$ (Fig. 7d). While (a) and (b) are representative of the axial (longitudinal) separation, (c) and (d) account for the lateral separation. The results are presented in Fig. 8. Note that the hydrodynamic effects become more pronounced when the swimmers are in the preferential plane (here, y - z plane) due to the typical nature of the flow field generated by these swimmers (multimedia available online). Consequently, the lateral outward drift is more pronounced for (c) and (d), although there is also an outward drift for (a) and (b), see Fig. 8d. The configurations (a) and (b) are quite similar and so are the hydrodynamic interactions between them. In fact, they differ only by magnitude, where (a) can be perceived as a future event of (b), when the axial approach brings these swimmers close enough to

each other by $1bl$. Similarly, the configurations (c) and (d) are also very similar and differ only by magnitude, where (d) can potentially be perceived as a future event of (c) when the lateral outward drift sets these swimmers apart further by a spacing of an additional $1bl$.

As discussed previously, the swimming trajectory of a swimmer is quite similar to a fractal (geometric) structure. Taking a close look at the phase plot of swimmer $s1$ (blue curve in Fig. 8a), we observe three different length scales. The wiggling (helical) motion of the soft robotic swimmer with every actuation cycle is manifested in the smallest length scale (a half-circle). The largest length scale is the outcome of hydrodynamic interactions between the individual swimmers when they revolve around each other. The third length scale (cloud-like structure) is in between the other two extreme length scales.

While the swimming trajectory of the swimmer $s1$ for

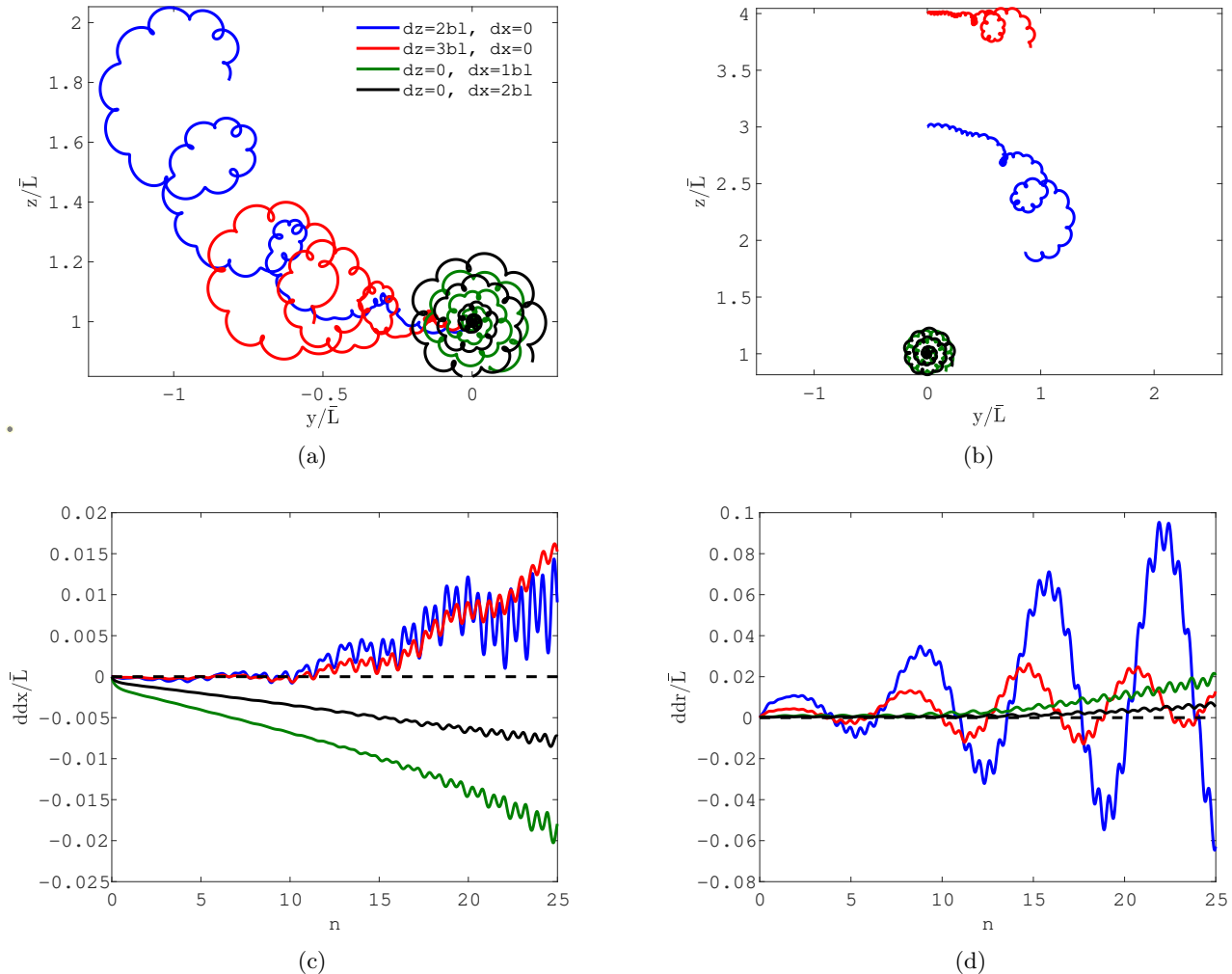


FIG. 8: (a) Swimming trajectories of (a) s1 and (b) s2, and variation of normalized (c) longitudinal and (d) lateral separation over each swimming cycle. Note that the swimmers gradually drift laterally outward in a sinusoidal pattern. This is apparent from the curve’s bias, which shows an increasing net area as the number of swimming cycles increases.

the configuration in Fig. 7d is similar to that for the configuration in Fig. 7c, the hydrodynamic interactions and the rotational rearrangement are higher in magnitude (see red and blue curves in Fig. 8a). Therefore, all the three length scales grow in magnitude as does ddr/\bar{L} in Fig. 8d, although they still exhibit a fractal structure in their swimming trajectories. The swimming trajectories of swimmer s2 for the aforementioned four distinct starting configurations are schematically plotted in Fig. 8b. Clearly, the blue trajectory is the outcome when they are placed $2bl$ apart along the lateral direction, while the red trajectory represents the phase plot of swimmer s2 when their (initial) separation is $3bl$.

When the swimmers have an axial separation (and no lateral separation), the hydrodynamic interactions seem to be the least, although they still influence the swimming kinematics of each other. Therefore, the swimmers

still exhibit the smallest length scale, although the other two length scales are insignificant (see Figs. 8a and 8b). However, there is important spatiotemporal manifestations even during these cases. It turns out they will approach each other which might be caused by the front swimmer causing a reduction of drag forces for the follower swimmer. Therefore, this helps the latter to swim faster and move closer to the leading swimmer with every swimming cycle. Hence, they behave much like attractors, wherein the normalized distance between them gradually decreases with the number of actuation cycles (as shown in Fig. 8c).

It is important to note that as they come closer to each other, they also start interacting differently because they now see each other in a more pronounced manner causing them to start moving laterally outward (although quite minimally; see Fig. 8d), and this is clearly mani-

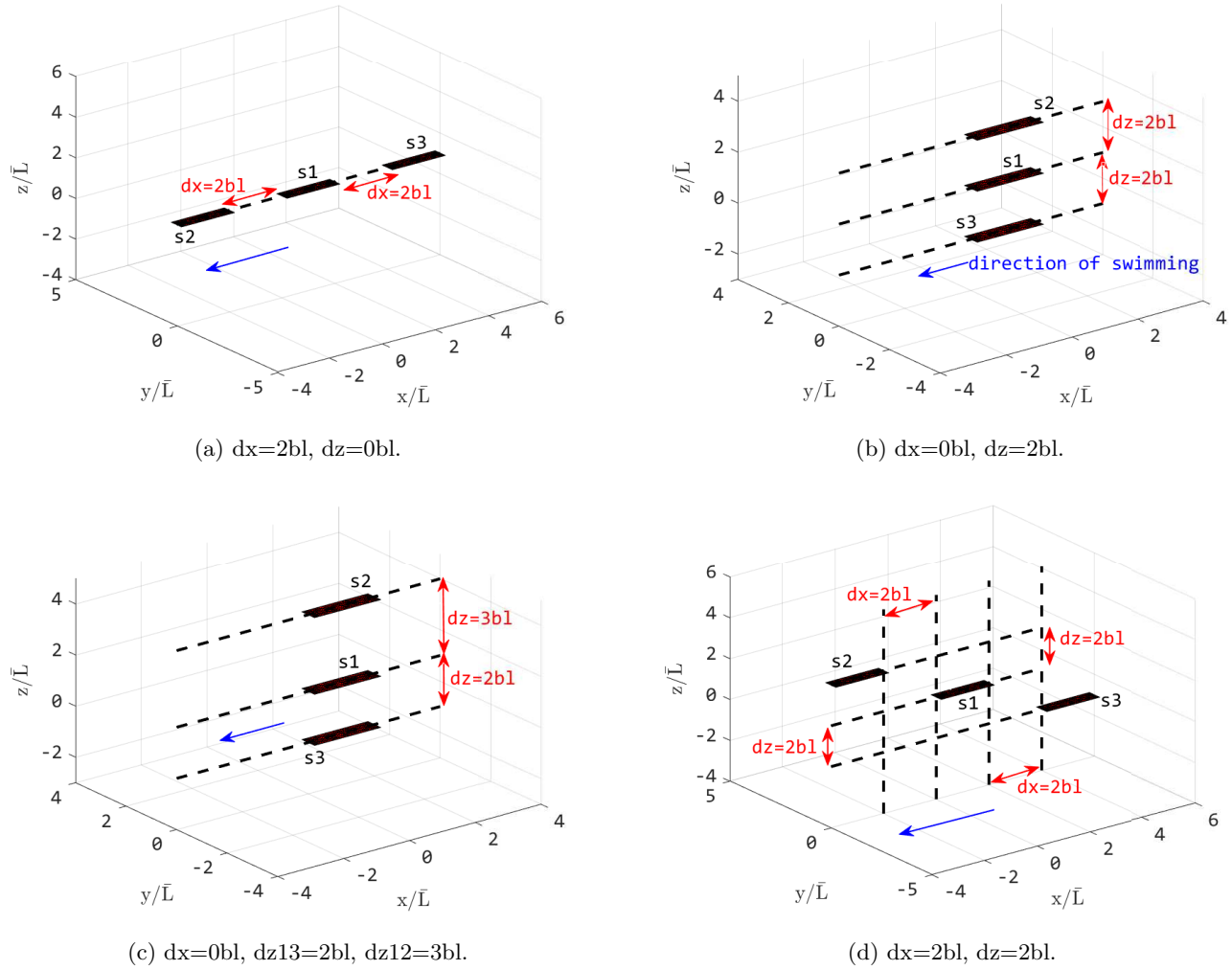


FIG. 9: Schematic representation of different initial (spatial) configurations of three soft robotic swimmers. Swimmers s_1 , s_2 , and s_3 are identified in black. The direction of swimming is shown in blue. The separation between the swimmers is denoted (dx and/or dz) in red. The front of swimmer s_1 in all subplots is located at $(x,y,z) = (0,0,\bar{L})$; for (a) and (b): (multimedia available online).

fested in the increasing oscillatory pattern after $n=15$ in Figs. 8c and 8d. However, when there is a lateral separation (and no axial separation) between the swimmers, the hydrodynamic interactions are most prominent. Therefore, the individual swimmers revolve around each other and have the most circular distance covered during their swimming trajectory. Typically, they behave as repellers and the normalized lateral distance between them sinusoidally varies (with a time-average increase) with an increasing number of cycles (see Fig. 8d). Importantly, the cumulative area under all the curves in 8d is positive (irrespective of whether dr/\bar{L} varies sinusoidally or increases almost linearly with small oscillations). This means that the swimmers drift apart with every actuation cycle.

Briefly, after analyzing the fluid-mediated hydrodynamic interactions between two soft robotic swimmers and also studying the influence of different starting con-

figurations, the following picture emerges: the out-of-plane swimmers come closer to each other (attractors) and their axial separation decreases; essentially, the hydrodynamic interactions gradually increase, until they can potentially lie in one single (preferential plane). Once in the in-plane configuration, the swimmers start drifting laterally outwards to reduce the hydrodynamic interactions (repellers) until they do not see each other anymore (theoretically, at infinity). This gradual transition from an out-of-plane configuration to slowly merging to a preferred in-plane configuration seems to be the hallmark of emergent behavior of swarms of helical soft robotic swimmers. Although we have, until now, shown this (emergent) behavior only for two swimmers, this hypothesis likely holds true for larger systems (e.g., swarms).

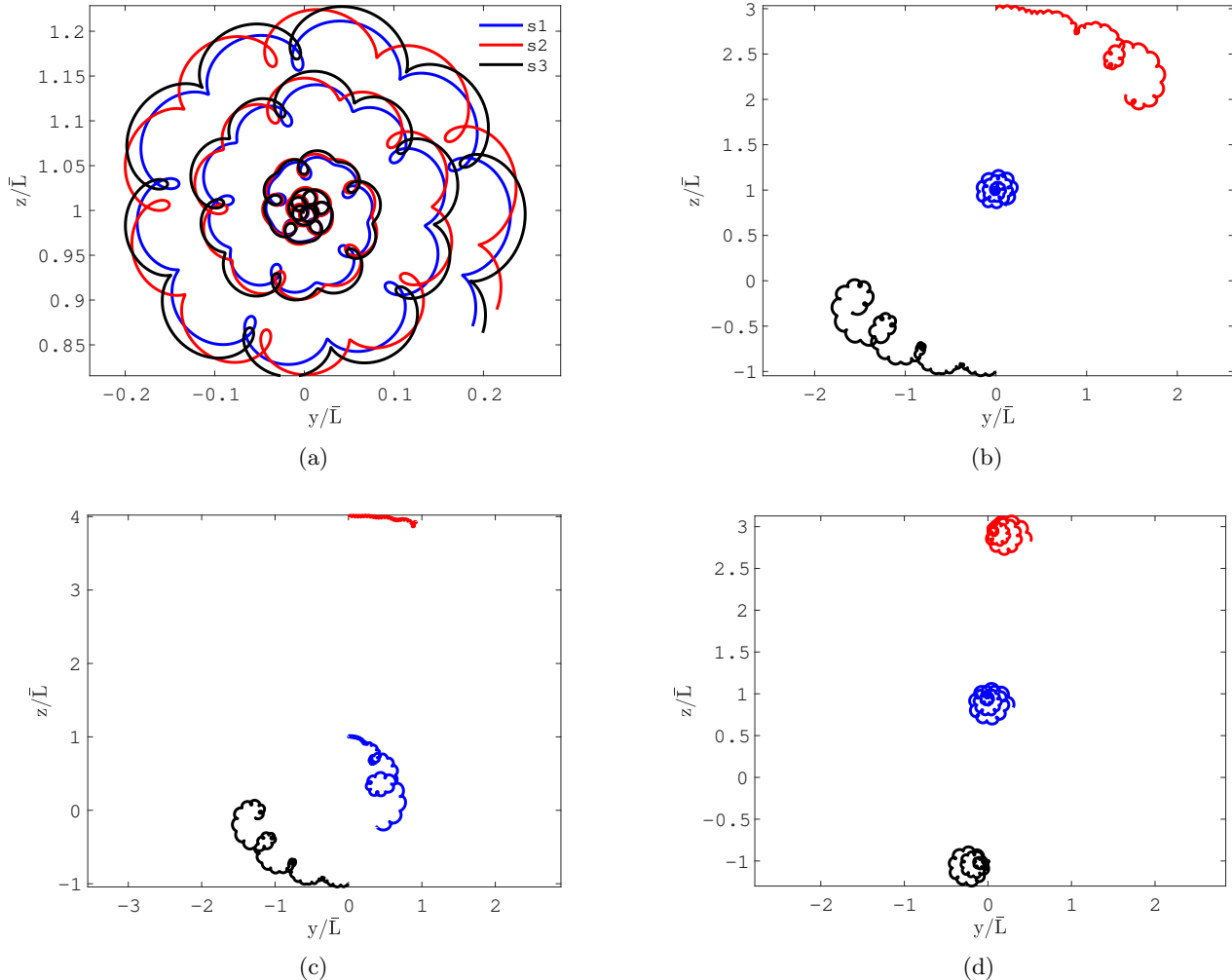


FIG. 10: Swimming trajectories of three swimmers for different spatial configurations in (a), (b), (c), and (d), corresponding to the starting configurations shown in Figs. 9(a), 9(b), 9(c), and 9(d), respectively (multimedia available online).

D. Emergent behavior: 3 swimmers

Next, we study the spatiotemporal patterning and emergent behavior of three swimmers. Like before, we consider three similar helical soft robotic swimmers (s_1 , s_2 , and s_3) for four distinct starting configurations: (a) when they are axially separated by $2bl$ [Fig. 9a (multimedia online)], (b) when they are laterally separated by $2bl$ [Fig. 9b (multimedia online)], (c) when they are laterally separated but asymmetrically by $2bl$ and $3bl$ (Fig. 9c), and (d) when they are diagonally arranged as shown in Fig. 9d; the phase plots of these four cases for $n=25$ swimming cycles are plotted in Figs. 10a-10d, respectively.

When the swimmers are axially separated with no lateral separation initially, the hydrodynamic interactions between them are minimal. This is intuitive from our previous analysis of the two swimmer swarms. Therefore,

their phase plots (swimming trajectories) look quite similar to each other (see Fig. 10a). Furthermore, thanks to negligible fluidic cross-talk between the individual swimmers in this configuration, there exists only one predominant length scale (i.e., the smallest wiggling helical motion manifested length scale). The fractal structure is missing, and so is the largest length scale of circular path traversal, because the centers of rotation of all the three swimmers are collinear in the axially separated configuration at $(y,z)=(0,\bar{L})$. Nevertheless, this configuration (if continued for several hundreds of actuation or swimming cycles) would gradually result in an in-plane (i.e., preferential plane) configuration - maintaining the hallmark emergent behavior of these helical soft robotic swimmer collectives (see Fig. 11). Finally, upon a close look into the swimming trajectories, we observe a laterally outward trajectory, much like a spiral curve with increasing radius (reminiscent of the famous Fermat's spiral).

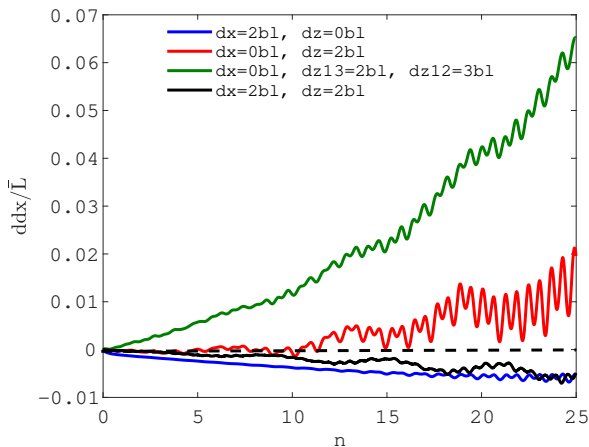


FIG. 11: Variation of normalized change in axial separation between swimmers s2 and s3 over each swimming cycle for different configurations of three swimmers depicted in Fig. 9.

Furthermore, there appears to be an increasing phase lag between the red (s2) and the blue/black swimmer (s1/s3). Our reasoning for this observation again goes back to our previous study on two axially separated swimmer. Here, swimmer s2 is the leading swimmer, and faces the maximum fluidic resistance with the trailing swimmers s1 and s3 having lower drag forces. Hence, s1 and s3 approach s2 aiming to minimize their axial separation. Hence, there is a phase lag in the swimming trajectory of swimmer s2 (in red) compared to that of swimmers s1 (in blue) or s3 (in black), both of which are similar without noticeable phase lag.

In Fig. 10b, we observe the phase plot of laterally separated symmetric in-plane three swimmer swarms. This is typically the situation when the hydrodynamic interactions are maximal. Consequently, the outer swimmers s2 and s3 start revolving around the central swimmer (s1) and drift radially outward. Owing to the symmetry of the configuration, the phase plot of the outer swimmers are quite similar. Additionally, they exhibit a fractal structure as discussed previously. The outer swimmers eventually drift apart laterally outwards until they negligibly interact any further (theoretically, at infinity). However, they still have a sinusoidally varying lateral distance between them (that has a positive area under the curve) with every swimming/actuation cycle. While the swimmer s2 (in red) travels initially rightward, the swimmer s3 (in black) traverses leftward in the same way due to the nature of the flow field around these swimmers (multimedia available online).

The configuration of the soft robotic swimmers in Fig. 10c is similar to Fig. 10b, apart from the fact that the outer swimmers are not symmetrically placed initially. Therefore, all the three swimmers start revolving along their distinct (fractal-like) swimming paths (in spiral trajectories) radially outward. All the swimmers revolve

clockwise in line with the surrounding flow field (multimedia available online). The hydrodynamic effects on the swimming trajectory of swimmer s2 are the least. Consequently, it revolves much less and has traversed a minimal path of revolution.

Finally, we investigate the configuration as schematically shown in Fig. 9d. These swimmers are initially placed in a diagonal manner. Here, it would be interesting to investigate whether their motion can be explained from a superposition of the axial motion of the swimmers (in case they do not have a lateral separation (Fig. 9a) and the lateral motion (in case they do not have an axial separation, as in 9b). Therefore, we plot their axial behaviour in Fig. 11. However, we notice that this is not the case. In both the axial and lateral direction they interact much less than in the case they would only have axial or lateral separation. Fig. 10d is not the same as Fig. 10b. In addition, their axial motion is not the same as that of the case of Fig. 9a. This is simply because of their reduced hydrodynamic interactions owing to their initial distance being larger than in the case of only lateral or axial separation.

E. Influence of aspect ratio

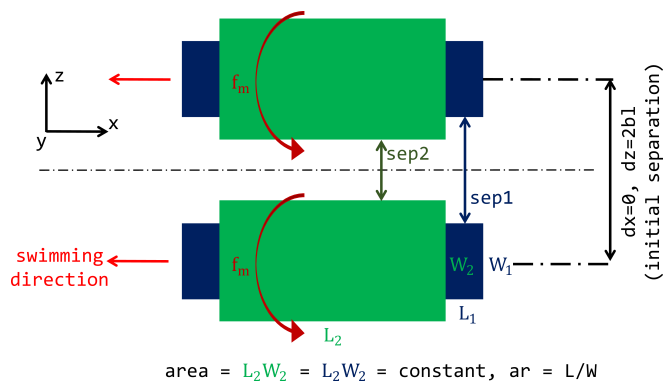


FIG. 12: Schematic representation of swimmers with different aspect ratios, yet having the same area. The swimmers have an initial lateral separation of $dz=2b1$, and axial separation of $dx=0$ irrespective of their aspect ratios. However, a higher ar (blue swimmer) has a larger lateral separation (sep1), and thus account for lower hydrodynamic interactions. The swimmers with a lower ar see each other more (due to lower value of sep2), and therefore, interact more through fluidic cross-talk. Please note that the difference between sep1 and sep2 is minimal compared to $dz=2b1$; i.e., $sep1-sep2 \ll 2b1$. Figure is for representation only, and not to scale.

Finally, we investigate the role of aspect ratio (ar) upon the hydrodynamic interactions between the soft robotic swimmers, which result in slightly different emergent behavior, phase plots, and spatiotemporal patterning. Here, the swimmer area (LW) is kept the same (for a

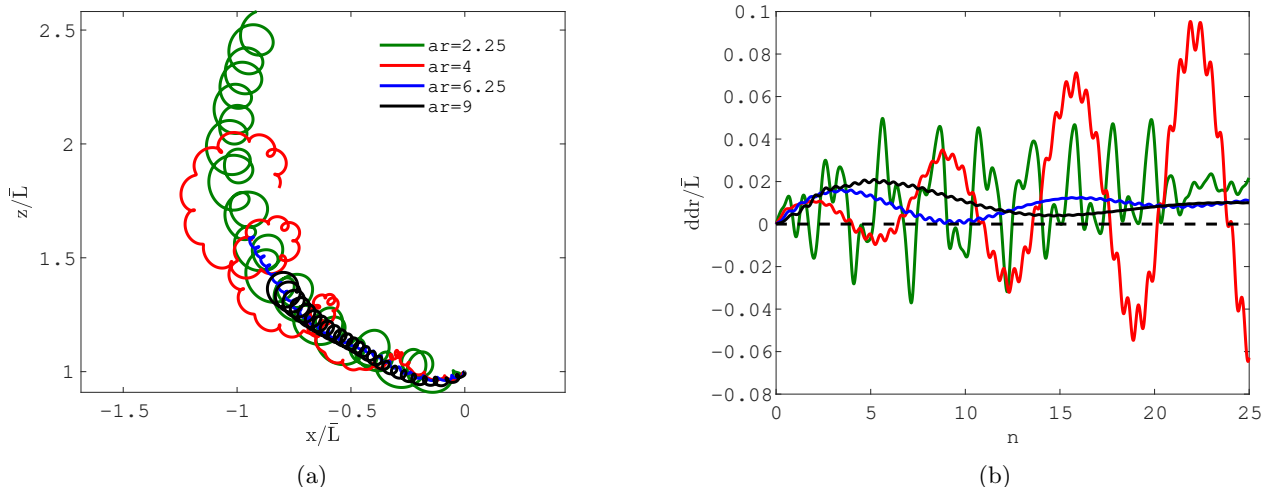


FIG. 13: (a) Phase plots and (b) variation of normalized lateral separation with number of swimming cycles of 2 swimmers for different aspect ratios.

uniform analysis), while ar is changed simply by varying the length L and width W systematically (see Fig. 12); and, $ar = L/W$. Furthermore, the characteristic body length \bar{L} is fixed by virtue of its definition, and is the square root of the swimmer area (see Fig. 1). To investigate this further, we consider the configuration of two swimmers that are laterally separated by $dz=2bl$ (see Figs. 3, 7 and 8, having an ar of 4). The phase plot of swimmer $s1$ is represented in Fig. 13a, where we note that the case of $ar=4$ corresponds to the results shown in Fig. 8a. The normalized lateral separation between them as a function of number of cycles, n is plotted in Fig. 13b for different values of ar ranging from 2.25 to 9, where the swimmers with the ar value of 2.25 is less rectangular (and thus difficult to twist), while the ones with $ar=9$ can easily twist.

Hence, for the same initial spatial configuration ($dx=0bl$, $dz=2bl$), the swimmers with a higher aspect ratio (but same area, and therefore, lower width W) has a higher lateral separation, effectively leading to lower hydrodynamic interactions (see Fig. 12). Therefore, the swimmers of $ar=9$ have a slightly higher separation (compared to swimmers of $ar=2.25$) and they interact less through fluidic cross-talk). The phase plot of swimmer $s1$ for $ar=2.25$ has the highest circular distance covered for the same number of swimming cycles ($n=25$), compared to that of swimmer $s1$ for $ar=9$ that has the lowest distance (see Fig. 13a).

III. CONCLUSION

In conclusion, we report the emergent behavior, collective swimming, and spatiotemporal patterning of

magnetically actuated miniaturized helical soft robotic swarms consisting of 2 to 3 swimmers, where typically, the individual swimmers affect the swimming behavior of each other through long-range fluid-mediated non-reciprocal hydrodynamic interactions leading to far-from-equilibrium self-organizational behavior. When these swimmers are out of plane (i.e., they have a longitudinal separation), they gradually come closer to each other over each swimming cycle, thereby behaving as attractors. However, when they are in plane (i.e., no longitudinal separation, but only a lateral separation), they gradually move outward along a lateral direction (thereby behaving as repellers). Therefore, they evade any possibility of agglomeration (or clustering). Although we report our findings mostly for two and three swimmer configurations, our results can principally be extrapolated to larger systems (i.e., swarms) without any loss of generality.

ACKNOWLEDGEMENTS

The authors would like to thank the Center for Information Technology of the University of Groningen for their support and for providing access to the Habrok high-performance computing cluster. The work is carried out within the research program of the Centre for Data Science and Systems Complexity (DSSC), Faculty of Science and Engineering, University of Groningen.

CONFLICT OF INTEREST

The authors have no conflicts to disclose.

-
- [1] P. Q. Nguyen, N.-M. D. Courchesne, A. Duraj-Thatte, P. Praveschotinunt, and N. S. Joshi, Engineered living materials: prospects and challenges for using biological systems to direct the assembly of smart materials, *Advanced Materials* **30**, 1704847 (2018).
- [2] M. R. Shaebani, A. Wysocki, R. G. Winkler, G. Gompfer, and H. Rieger, Computational models for active matter, *Nature Reviews Physics* **2**, 181 (2020).
- [3] L. Ning, H. Zhu, J. Yang, Q. Zhang, P. Liu, R. Ni, and N. Zheng, Macroscopic, artificial active matter, *National Science Open* **3**, 20240005 (2024).
- [4] W. Zuo and Y. Wu, Dynamic motility selection drives population segregation in a bacterial swarm, *Proceedings of the National Academy of Sciences* **117**, 4693 (2020).
- [5] M. Tian, C. Zhang, R. Zhang, and J. Yuan, Collective motion enhances chemotaxis in a two-dimensional bacterial swarm, *Biophysical journal* **120**, 1615 (2021).
- [6] Y. Wu, Collective motion of bacteria in two dimensions, *Quantitative Biology* **3**, 199 (2015).
- [7] G. Gardi and M. Sitti, On-demand breaking of action-reaction reciprocity between magnetic microdisks using global stimuli, *Physical review letters* **131**, 058301 (2023).
- [8] G. Kokot and A. Snezhko, Manipulation of emergent vortices in swarms of magnetic rollers, *Nature communications* **9**, 2344 (2018).
- [9] E. Lushi, H. Wioland, and R. E. Goldstein, Fluid flows created by swimming bacteria drive self-organization in confined suspensions, *Proceedings of the National Academy of Sciences* **111**, 9733 (2014).
- [10] M. F. Hagan and A. Baskaran, Emergent self-organization in active materials, *Current opinion in cell biology* **38**, 74 (2016).
- [11] L. Yang and L. Zhang, Motion control in magnetic micro-robotics: From individual and multiple robots to swarms, *Annual Review of Control, Robotics, and Autonomous Systems* **4**, 509 (2021).
- [12] J. Chen, M. Gauci, W. Li, A. Kolling, and R. Groß, Occlusion-based cooperative transport with a swarm of miniature mobile robots, *IEEE Transactions on Robotics* **31**, 307 (2015).
- [13] C. Zimmermann, P. Herson, K. Neeves, and D. Marr, Multimodal microwheel swarms for targeting in three-dimensional networks, *Scientific reports* **12**, 5078 (2022).
- [14] X. Dong and M. Sitti, Collective formation and cooperative function of a magnetic microrobotic swarm., in *Robotics: Science and Systems* (2019).
- [15] B. Chaluvadi, K. M. Stewart, A. J. Sperry, H. C. Fu, and J. J. Abbott, Kinematic model of a magnetic-microrobot swarm in a rotating magnetic dipole field, *IEEE Robotics and Automation Letters* **5**, 2419 (2020).
- [16] F. N. P. Basualdo, G. Gardi, W. Wang, S. O. Demir, A. Bolopion, M. Gauthier, P. Lambert, and M. Sitti, Control and transport of passive particles using self-organized spinning micro-disks, *IEEE Robotics and Automation Letters* **7**, 2156 (2022).
- [17] R. Fujiwara, T. Kano, and A. Ishiguro, Self-swarming robots that exploit hydrodynamical interaction, *Advanced Robotics* **28**, 639 (2014).
- [18] M. R. Pac, A. M. Erkmén, and I. Erkmén, Control of robotic swarm behaviors based on smoothed particle hydrodynamics, in *2007 IEEE/RSJ International Conference on Intelligent Robots and Systems (IEEE, 2007)* pp. 4194–4200.
- [19] Y. Wang, S. Canic, G. Kokot, A. Snezhko, and I. Aranson, Quantifying hydrodynamic collective states of magnetic colloidal spinners and rollers, *Physical Review Fluids* **4**, 013701 (2019).
- [20] G. Kokot, D. Piet, G. M. Whitesides, I. S. Aranson, and A. Snezhko, Emergence of reconfigurable wires and spinners via dynamic self-assembly, *Scientific reports* **5**, 9528 (2015).
- [21] Y. B. Mitikiri, M. Silic, and K. Mohseni, Smoothed-particle-hydrodynamics for the control of robotic swarms, and parametric associations, *IEEE Transactions on Control of Network Systems* **8**, 1942 (2021).
- [22] W. Wang, G. Gardi, P. Magaretti, V. Kishore, L. Koenig, D. Son, H. Gilbert, Z. Wu, P. Harwani, E. Lauga, *et al.*, Order and information in the patterns of spinning magnetic micro-disks at the air-water interface, *Science Advances* **8**, eabk0685 (2022).
- [23] H. Xie, X. Fan, M. Sun, Z. Lin, Q. He, and L. Sun, Programmable generation and motion control of a snakelike magnetic microrobot swarm, *IEEE/ASME Transactions on Mechatronics* **24**, 902 (2019).
- [24] G. Kokot, G. V. Kolmakov, I. S. Aranson, and A. Snezhko, Dynamic self-assembly and self-organized transport of magnetic micro-swimmers, *Scientific reports* **7**, 14726 (2017).
- [25] W. T. Ashurst and W. G. Hoover, Microscopic fracture studies in the two-dimensional triangular lattice, *Physical Review B* **14**, 1465 (1976).
- [26] S. Succi, *The lattice Boltzmann equation: for fluid dynamics and beyond* (Oxford university press, 2001).
- [27] A. Alexeev, R. Verberg, and A. C. Balazs, Modeling the motion of microcapsules on compliant polymeric surfaces, *Macromolecules* **38**, 10244 (2005).
- [28] S. Liang, Y. Miao, X. Zhu, J. Wei, Q.-F. Zhan, X. Huang, and L. Zhang, Magnetic actuation of hollow swarming spheres for dynamic catalysis, *ACS Applied Materials & Interfaces* **13**, 11424 (2021).
- [29] K. Han, A. Sokolov, A. Glatz, and A. Snezhko, Manipulation of self-organized multi-vortical states in active magnetic roller suspensions, *Journal of Magnetism and Magnetic Materials* **589**, 171625 (2024).
- [30] F. Martínez-Pedrero, E. Navarro-Argemí, A. Ortiz-Ambríz, I. Pagonabarraga, and P. Tierno, Emergent hydrodynamic bound states between magnetically powered micropropellers, *Science advances* **4**, eaap9379 (2018).
- [31] D. Ehrenstein, Magnetic microdisks don't always reciprocate, *Physics* **16**, 135 (2023).
- [32] B. Wang, K. F. Chan, J. Yu, Q. Wang, L. Yang, P. W. Y. Chiu, and L. Zhang, Reconfigurable swarms of ferromagnetic colloids for enhanced local hyperthermia, *Advanced Functional Materials* **28**, 1705701 (2018).
- [33] W. Hu, G. Z. Lum, M. Mastrangeli, and M. Sitti, Small-scale soft-bodied robot with multimodal locomotion, *Nature* **554**, 81 (2018).
- [34] Z. Ren, R. Zhang, R. H. Soon, Z. Liu, W. Hu, P. R. Onck, and M. Sitti, Soft-bodied adaptive multimodal locomotion strategies in fluid-filled confined spaces, *Science advances* **7**, eabh2022 (2021).

- [35] X. Wang, G. Mao, J. Ge, M. Drack, G. S. Cañón Bermúdez, D. Wirthl, R. Illing, T. Kosub, L. Bischoff, C. Wang, *et al.*, Untethered and ultrafast soft-bodied robots, *Communications Materials* **1**, 67 (2020).
- [36] Z. Ye, L. Zheng, W. Chen, B. Wang, and L. Zhang, Recent advances in bioinspired soft robots: Fabrication, actuation, tracking, and applications, *Advanced Materials Technologies* , 2301862 (2024).
- [37] H. Zhou, C. C. Mayorga-Martinez, S. Pané, L. Zhang, and M. Pumera, Magnetically driven micro and nanorobots, *Chemical Reviews* **121**, 4999 (2021).
- [38] D. Quashie, P. Benhal, Z. Chen, Z. Wang, X. Mu, X. Song, T. Jiang, Y. Zhong, U. K. Cheang, and J. Ali, Magnetic bio-hybrid micro actuators, *Nanoscale* **14**, 4364 (2022).
- [39] B. Wang and Y. Lu, Multi-dimensional micro/nanorobots with collective behaviors, *SmartMat* , e1263 (2024).
- [40] R. Pramanik, R. Verstappen, and P. Onck, Magnetic-field-induced propulsion of jellyfish-inspired soft robotic swimmers, *Physical Review E* **107**, 014607 (2023).
- [41] R. Pramanik, R. Verstappen, and P. Onck, Nature-inspired miniaturized magnetic soft robotic swimmers, *Applied Physics Reviews* **11** (2024).
- [42] R. Pramanik, M. Park, Z. Ren, M. Sitti, R. Verstappen, and P. Onck, Computational and experimental design of fast and versatile magnet (2024), arXiv:2409.11215 [cs.RO].
- [43] S. Khaderi and P. Onck, Fluid–structure interaction of three-dimensional magnetic artificial cilia, *Journal of Fluid Mechanics* **708**, 303 (2012).
- [44] S. Namdeo, S. Khaderi, and P. Onck, Numerical modelling of chirality-induced bi-directional swimming of artificial flagella, *Proceedings of the Royal Society A: Mathematical, Physical and Engineering Sciences* **470**, 20130547 (2014).